J|A|C|S
ARTICLES
Published on Web 08/17/2002

Theoretical and Experimental Investigation of the Effect of Proton Transfer on the ^{27}Al MAS NMR Line Shapes of Zeolite−Adsorbate Complexes: An Independent Measure of Solid Acid Strength

Justin O. Ehresmann, Wei Wang, Bruno Herreros, Donat-Pierre Luigi, T. N. Venkatraman, Weiguo Song, John B. Nicholas,† and James F. Haw*

Contribution from the Loker Hydrocarbon Research Institute and Department of Chemistry, University of Southern California, University Park, Los Angeles, California 90089-1661

Received October 11, 2001. Revised Manuscript Received May 3, 2002

Abstract: Assessing the degree of proton transfer from a Brønsted acid site to one or more adsorbed bases is central to arguments regarding the strength of zeolites and other solid acids. In this regard certain solid-state NMR measurements have been fruitful; for example, some ^{13}C, ^{15}N, or ^{31}P resonances of adsorbed bases are sensitive to protonation, and the ^{1}H chemical shift of the Brønsted site itself reflects hydrogen bonding. We modeled theoretically the structures of adsorption complexes of several bases on zeolite HZSM-5, calculated the quadrupole coupling constants (Q_{cc}) and asymmetry parameters (η) for aluminum in these complexes and then in turn simulated the central transitions of their ^{27}Al MAS NMR spectra. The theoretical line width decreased monotonically with the degree of proton transfer, reflecting structural relaxation around aluminum as the proton was transferred to a base. We verified this experimentally for a series of adsorbed bases by way of single-pulse MAS and triple quantum MQMAS ^{27}Al NMR. The combined theoretical and experimental approach described here provides a strategy by which ^{27}Al data can be applied to resolve disputed interpretations of proton transfer based on other evidence.

Introduction

The most fundamental problem in the chemistry of solid acids is determining the degree of proton transfer from a Brønsted acid site to various adsorbed bases. In this regard solid-state NMR studies of adsorbed probe molecules have been very useful.[1−12] Many of these are also used to probe Lewis acid sites, but we consider only Brønsted sites in this contribution. For example, $P(CH_3)_3$ is readily protonated by the Brønsted sites of aluminosilicate zeolites to form $HP(CH_3)_3^+$, and the ^{31}P NMR spectrum measured using magic-angle spinning (MAS) reflects proton transfer through a chemical shift and a resolved ^{1}H−^{31}P scalar coupling.[1,2] An alternative and sometimes complementary strategy relies on the sensitivity of the ^{1}H chemical shift to the strength of the hydrogen bond formed between the adsorbed base and the Brønsted acid site,[13,14] much as in studies of hydrogen bonds in solution.[15] Finally, some NMR experiments have measured through-space dipolar couplings between one or more spins on the base and the Brønsted site proton to reach conclusions about proton transfer.[16−18]

In this contribution we describe another, entirely general NMR method to evaluate the degree of proton transfer from the Brønsted site of an aluminosilicate zeolite to an adsorbed base. It has long been recognized that the ^{27}Al resonance of framework sites of zeolites is narrow when the material is saturated with water, but that signal greatly broadens upon dehydration. When the acid-site proton is transferred to a cluster of several water molecules, the associated aluminum adopts a nearly tetrahedral environment, but when the proton is on the

* To whom correspondence should be addressed. E-mail: jhaw@usc.edu.
† Current address: Genentech, Inc. 1 DNA Way, South San Francisco, CA, 94065.

(1) Rothwell, W. P.; Shen, W.; Lunsford, J. H. *J. Am. Chem. Soc.* **1984**, *106*, 2452−2453.
(2) Lunsford, J. H.; Rothwell, W. P.; Shen, W. *J. Am. Chem. Soc.* **1985**, *107*, 1540−1547.
(3) Haw, J. F.; Chuang, I.-S.; Hawkins, B. L.; Maciel, G. E. *J. Am. Chem. Soc.* **1983**, *105*, 7206−7207.
(4) Kao, H. M.; Liu, H. M.; Jiang, J. C.; Lin, S. H.; Grey, C. P. *J. Phys. Chem. B* **2000**, *104*, 4923−4933.
(5) Kao, H. M.; Grey, C. P. *J. Am. Chem. Soc.* **1997**, *119*, 627−628.
(6) Baltusis, L.; Frye, J. S.; Maciel, G. E. *J. Am. Chem. Soc.* **1986**, *108*, 7119−7120.
(7) Xu, T.; Munson, E. J.; Haw, J. F. *J. Am. Chem. Soc.* **1994**, *116*, 1962−1972.
(8) Barich, D. H.; Nicholas, J. B.; Xu, T.; Haw, J. F. *J. Am. Chem. Soc.* **1998**, *120*, 12342−12350.
(9) Haw, J. F.; Zhang, J. H.; Shimizu, K.; Venkatraman, T. N.; Luigi, D. P.; Song, W. G.; Barich, D. H.; Nicholas, J. B. *J. Am. Chem. Soc.* **2000**, *122*, 12561−12570.
(10) Osegovic, J. P.; Drago, R. S. *J. Phys Chem. B* **2000**, *104*, 147−154.
(11) Rakiewicz, E. F.; Peters, A. W.; Wormsbecher, F.; Sutovich, K. J.; Mueller, K. T. *J. Phys. Chem. B* **1998**, *102*, 2890−2896.
(12) Trout, B. L.; Suits, B. H.; Gorte, R. J.; White, D. *J. Phys Chem. B* **2000**, *104*, 147−154.
(13) White, J. L.; Beck, L. W.; Haw, J. F. *J. Am. Chem. Soc.* **1992**, *114*, 6182−6189.
(14) Paze, C.; Zecchina, A.; Spera, S.; Corma, A.; Merlo, E.; Spano, G.; Girotti, G. *Phys. Chem. Chem. Phys.* **1999**, *1*, 2627−2629.
(15) Jeffrey, G. A. *An Introduction to Hydrogen Bonding*; Oxford University Press: New York, 1997.
(16) Heeribout, L.; Doremieux-Morin, C.; Nogier, J. P.; Vincent, R.; Fraissard, J. *Microporous Mesoporous Mater.* **1998**, *24*, 101−112.
(17) Batamack, P.; Doremieux-Morin, C.; Fraissard, J.; Feude, D. *J. Chem. Phys.* **1991**, *95*, 3790−3796.
(18) Doremieux-Morin, C.; Heeribout, L.; Dumousseaux, C.; Fraissard, J.; Hommel, H.; Legrand, A. P. *J. Am. Chem. Soc.* **1996**, *118*, 13040−13045.

10.1021/ja012336u CCC: $22.00

acid site, the aluminum environment is distorted toward trigonal. Since ^{27}Al ($I = {}^5/_2$) is a half-integer quadrupole, the electrostatic field gradient resulting from distortion produces a significant quadrupolar coupling constant (Q_{cc}), and even the central ($+{}^1/_2 \rightleftarrows -{}^1/_2$) transition can be too broad for observation at moderate field strengths using magic-angle spinning.[19,20] Thus, the ^{27}Al signal of dehydrated zeolite HZSM-5 (proton form) is essentially invisible in a standard MAS NMR experiment,[21] but that of dehydrated NaZSM-5 (sodium-exchanged form) is relatively narrow, even at moderate fields.[22]

We carried out a systematic, combined theoretical and experimental study of the effect of proton donation on the ^{27}Al MAS line shape of zeolite HZSM-5, supplemented by MQMAS measurements for the two cases where the quadrupole coupling constant was small enough for its application. We used cluster models of the zeolite Brønsted site and density functional theory to model the geometries of adsorption complexes of several bases with widely differing gas-phase proton affinities. In the case of $P(CH_3)_3$ we found two states corresponding to proton transfer to the base (the lower-energy state observed experimentally) and a higher-energy state with weak hydrogen bonding but no proton transfer. Proton transfer was also observed theoretically with pyridine but not with acetone or nitromethane. We used these DFT cluster models[23] to calculate theoretically the quadrupole coupling constants (Q_{cc}) and asymmetry parameters (η) for ^{27}Al.[24,25] These values were in turn used to simulate the ^{27}Al MAS spectrum of the central transition under MAS conditions[26] for comparison with experiment.

The overall agreement between experiment and theory is remarkable. The narrow ^{27}Al resonances observed experimentally for the pyridine and $P(CH_3)_3$ complexes of zeolite HZSM-5 reproduce the essential character of the theoretical line shapes. In the case of $P(CH_3)_3$, the existence of a second minimum corresponding to no proton transfer allowed a direct comparison between experiment and two very different theoretical predictions. Very broad, essentially unobservable lines were observed experimentally for HZSM-5 complexes of either acetone or nitromethane. Theoretical calculations show that this was indeed the expected outcome, given the low degree of proton transfer and, hence, distortion of Al away from tetrahedral coordination.

The ^{27}Al MAS line shape, interpreted as necessary with the aid of theory, is a quantitative probe of structural relaxation accompanying proton transfer from a zeolitic Brønsted site to an adsorbate. This probe is independent of other spectroscopic measures of proton transfer, such as ^{1}H isotropic shift or dipolar line shapes. Thus, in cases where consensus cannot be reached on the degree of proton transfer using other spectroscopic probes, the line shape of the ^{27}Al central transition may provide definitive answers.

Experimental Section

Materials and Reagents. Acetone-2-^{13}C (99% ^{13}C) was purchased from Cambridge Isotopes. Other reagents were purchased from Aldrich and were purified using standard laboratory techniques. Zeolite HZSM-5 (Si/Al = 15) was obtained from Zeolyst.

Sample Preparation and MAS NMR. All samples were prepared using a shallow-bed CAVERN apparatus.[27] Typically 0.2 g of zeolite was loaded into the CAVERN, which was then connected to a vacuum line. The catalyst was first heated to a final temperature of 773 K with a heating rate of about 0.3 K/min. The catalyst was kept at the final temperature for 4 h under vacuum and then for 1 h at a final pressure of less than 5×10^{-5} Torr. Adsorption of volatile reagents (typically one equivalent for each Bronsted acid site) was carried out at room temperature with the exception of acetone, which required reduced temperature to prevent dimerization to mesityl oxide, a stronger base. Samples were loaded into 5-mm zirconia rotors after adsorption, and the rotor was capped within the CAVERN.

Conventional ^{27}Al MAS spectra were acquired on a Chemagnetics CMX 360 (8.46 T) spectrometer equipped with a modified Chemagnetics 5-mm MAS probe, whereas the MQMAS studies were performed on a Varian-Chemagnetics Infinity-plus 300 (7.05 T) using the same probe. All ^{27}Al signals are referenced to external aqueous $Al(NO_3)_3$. This sample was also used to calibrate the 90° flip for nonselective irradiation of all aluminum transitions. ^{27}Al MAS spectra of all zeolite samples were acquired using a 15° flip angle; 10000 scans were accumulated using a 3-s pulse delay. The MAS spinning speed was 7.2 kHz. The triple quantum MQMAS spectra were acquired using a two-pulse sequence in conjunction with a selective $\pi/2$ *z*-filter as has been described previously.[28,29] Multiple quantum excitation and conversion pulses were carried out at a radio frequency field strength corresponding to a nutation rate of 76 kHz; 256 $t1$ points were collected, each consisting of 216 transients with a data length of 512 points followed by a 1-s recycle delay. Prior to processing the $t1$ dimension was zero-filled to 1024 data points.

Theoretical Geometries. The geometries of all the zeolite models and complexes were optimized using the density functional theory (DFT) with $(H_3SiO)_3SiOHAl(OSiH_3)_3$ as the zeolite model.[30] During the optimizations the Cartesian positions of the terminal silyl groups were held fixed in the crystallographic positions.[31] We used the hybrid B3LYP[32] exchange-correlation functional, which includes the Hartree−Fock (HF) exchange in a parametrized way. The accuracy of this functional for bond distances is well established.[33] We used the polarized valence double-ζ (DZVP2) basis sets of Godbout and co-workers[34] for all the geometry optimizations. The orbital basis set used six *d* functions. We used Gaussian98 for all calculations.[35]

^{27}Al Shielding Calculations. ^{27}Al absolute shieldings were calculated for all of the models described above using the GIAO method[36] at the restricted Hartree−Fock (RHF) level with a tzp basis set.[37]

^{27}Al Quadrupole Parameter Calculations. In general, we followed the work of Koller et al.[24] on the quantum-chemical computation of the electric field gradient (EFG). EFG tensors were calculated using the PRISM algorithm[38] as implemented in Gaussian 98 at both the RHF and B3LYP levels of theory with Ahlrich's tzp large basis sets.[39] These tensors were diagonalized to yield the principal components, converted

(19) Fyfe, C. A.; Bretherton, J. L.; Lam, L. Y. *J. Am. Chem. Soc.* **2001**, *123*, 5285−5291.
(20) Fyfe, C. A.; Bretherton, J. L.; Lam, L. Y. *Chem. Commun.* **2000**, 1575−1576.
(21) Ernst, H.; Freude, D.; Wolf, I. *Chem. Phys. Lett.* **1993**, *212*, 588−596.
(22) Hunger, M.; Horvath, T. *Ber. Bunsen-Ges. Phys. Chem, Chem. Phys.* **1995**, *99*, 1316−1320.
(23) Haw, J. F.; Nicholas, J. B.; Xu, T.; Beck, L. W.; Ferguson, D. B. *Acc. Chem. Res.* **1996**, *29*, 259−267.
(24) Koller, H.; Meijer, E. L.; van Santen, R. A. *Solid State NMR* **1997**, *9*, 165−175.
(25) Bryant, P. L.; Harwell, C. R.; Mrse, A. A.; Emery, E. F.; Gan, Z. H.; Caldwell, T.; Reyes, A. P.; Kuhns, P.; Hoyt, D. W.; Simeral, L. S.; Hall, R. W.; Butler, L. G. *J. Am. Chem. Soc.* **2001**, *123*, 12009−12017.
(26) Kundla, E.; Samoson, A.; Lippmaa, E. *Chem. Phys. Lett.* **1981**, *83*, 229−232.
(27) Xu, T.; Haw, J. F. *Top. Catal.* **1997**, *4*, 109−118.
(28) Medek, A.; Harwood, J. S.; Frydman, L. *J. Am. Chem. Soc.* **1995**, *117*, 12779−12787.
(29) Amoureux, J. P.; Fernandez, C.; Steuernagel, S. *J. Magn. Reson.* **1996**, *123*, 116.
(30) Stave, M. S.; Nicholas, J. B. *J. Phys. Chem.* **1995**, *99*, 15046−15061.
(31) van Koningsveld, H.; van Bekkum, H.; Jansen, J. C. *Acta Crystallogr.* **1987**, *B43*, 127−132.
(32) Becke, A. D. *J. Chem. Phys.* **1993**, *98*, 5648−5652.
(33) Ma, B. Y.; Lii, J. H.; Schaefer, H. F.; Allinger, N. L. *J. Phys. Chem.* **1996**, *100*, 8763−8769.
(34) Godbout, N.; Salahub, D. R.; Andzelm, J.; Wimmer, E. *Can. J. Chem.* **1992**, *70*, 560−571.

from au to V/Å^2 and then were used to calculate the theoretical quadrupolar coupling constant (Q_{cc}) and the asymmetry parameter (η) for ^{27}Al. These are defined as:

$$Q_{cc} = \frac{e^2 V_{ZZ} Q}{h} \quad (1)$$

$$\eta = \frac{|V_{YY} - V_{XX}|}{V_{ZZ}} \quad (2)$$

V_{zz} is the largest component of the EFG, and Q is the quadrupole moment (14 fm^2 for ^{27}Al). The asymmetry parameter is such that $1 \geq \eta \geq 0$.

^{27}Al MAS NMR Line Shape Simulations. ^{27}Al MAS spectra of the central transition were calculated[40] using the computed quadrupolar parameters by integrating eq 5 of the work by Lippmaa and co-workers[26] over the angles α and β in an iterative manner (360 steps over α and 1000 steps over β for a total of 360 000 iterations). For each value of $\nu(\alpha,\beta)$ in the iteration process, intensities $I(\nu)$ were accumulated using $I(\nu) = \sin \beta$.

Results

Complex Geometries. We optimized the geometries of our neutral and deprotonated (anionic) zeolite models, and the complexes formed with nitromethane, acetone, trimethylphosphine, and pyridine. The optimized geometry for the acetone complex has been reported earlier,[8,23] and will not be discussed in detail here. For comparison to values reported below, the experimental proton affinity of acetone is 194 kcal/mol. The B3LYP/DZVP2 optimized geometry of the nitromethane complex CH_3NO_2·HZ is shown in Figure 1a. Nitromethane is the weakest base of the molecules studied here (experimental proton affinity = 180 kcal/mol) and thus forms the weakest hydrogen bond with the zeolite proton. However, the hydrogen bond strength is still quite large, being 11.2 kcal/mol (ΔE without correction for basis set superposition error (BSSE)). The distance between the proton and the nearest oxygen on nitromethane is 1.68 Å, also indicative of a strong hydrogen bond. The zeolite O−H distance is 1.00 Å, slightly lengthened from the value obtained for the isolated zeolite (0.97 Å), due to the formation of the hydrogen bond. The distance between Al and the hydroxyl O is 1.82 Å, whereas this bond length is 1.83 Å in the bare zeolite. While we do not expect proton transfer from the zeolite to nitromethane, due to the latter's weak basicity, the case is much different for pyridine (Figure 1b). The experimental proton affinity of pyridine is 222 kcal/mol. The optimization of the pyridine complex PyH^+·Z^- started with the proton on the zeolite. During the course of the optimization, the proton was transferred to pyridine, resulting in the zwitterionic complex between protonated pyridine and the zeolite anion. The O−H hydrogen bond length is 1.58 Å, consistent with a large hydrogen bond energy of 23.5 kcal/mol. Whereas the central O of the zeolite is no longer protonated, the Al−O distance is much shorter (1.74 Å). This distance is similar to the value we obtain from the optimization of the bare zeolite anion (1.72 Å). The N−H bond length on pyridine is 1.07 Å, whereas it is 1.02 Å in isolated protonated pyridine optimized at the same level of theory. Thus, there is some N−H bond lengthening due to the hydrogen bond.

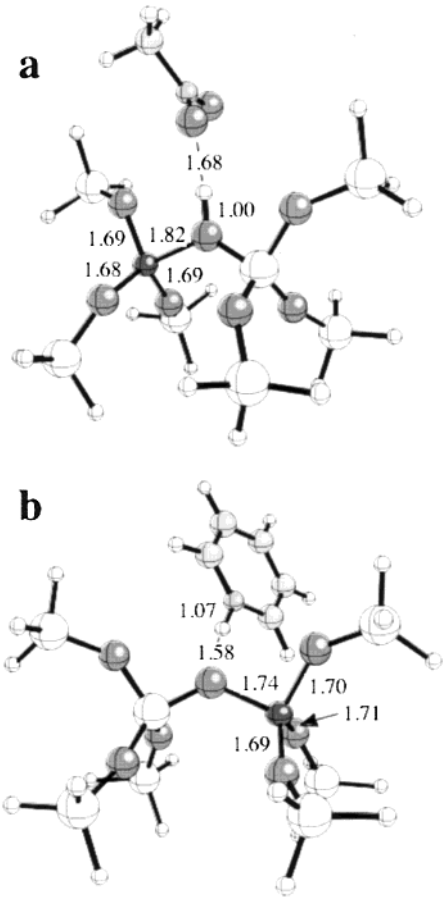

Figure 1. B3LYP/DZVP2 optimized geometries of (a) CH_3NO_2·HZ and (b) PyH^+·Z^-. Selected distances in Å are shown.

We have optimized many complexes between zeolite models and basic probe molecules. In some cases the adsorbate becomes protonated, and in some cases it does not. Figure 2 shows two geometries from complexes formed by the zeolite model and $P(CH_3)_3$. This is the only adsorbate for which we have been able to obtain stable complexes in both the protonated and unprotonated states. The gas-phase proton affinity of $P(CH_3)_3$ is 229 kcal/mol. In the neutral complex, $(CH_3)_3P$·HZ, the P of $P(CH_3)_3$ coordinates with the proton at 2.10 Å. While this distance is larger than the other hydrogen bonding distances we discussed earlier, the large size of P necessitates a longer distance, even if the hydrogen bond is strong. For $P(CH_3)_3$, the hydrogen bond energy is 11.1 kcal/mol, clearly consistent with a strong hydrogen bond. Also consistent with this interpretation, is the O−H distance of 1.05 Å, considerably longer than the 0.97 Å predicted for the bare zeolite. Figure 2b shows the

(35) Frisch, M. J.; Trucks, G. W.; Schlegel, H. B.; Scuseria, G. E.; Robb, M. A.; Cheeseman, J. R.; Zakrzewski, V. G.; Montgomery, J. A., Jr.; Stratmann, R. E.; Burant, J. C.; Dapprich, S.; Millam, J. M.; Daniels, A. D.; Kudin, K. N.; Strain, M. C.; Farkas, O.; Tomasi, J.; Barone, V.; Cossi, M.; Cammi, R.; Mennucci, B.; Pomelli, C.; Adamo, C.; Clifford, S.; Ochterski, J.; Petersson, G. A.; Ayala, P. Y.; Cui, Q.; Morokuma, K.; Malick, D. K.; Rabuck, A. D.; Raghavachari, K.; Foresman, J. B.; Cioslowski, J.; Ortiz, J. V.; Stefanov, B. B.; Liu, G.; Liashenko, A.; Piskorz, P.; Komaromi, I.; Gomperts, R.; Martin, R. L.; Fox, D. J.; Keith, T.; Al-Laham, M. A.; Peng, C. Y.; Nanayakkara, A.; Gonzalez, C.; Challacombe, M.; Gill, P. M. W.; Johnson, B. G.; Chen, W.; Wong, M. W.; Andres, J. L.; Head-Gordon, M.; Replogle, E. S.; Pople, J. A. *Gaussian 98*, revision A.4; Gaussian, Inc.: Pittsburgh, PA, 1998.
(36) Ditchfield, R. *Mol. Phys.* **1974**, *27*, 789−807.
(37) Schafer, A.; Huber, C.; Ahlrichs, R. *J. Chem. Phys.* **1994**, *100*, 5829−5834.
(38) Johnson, B. G.; Gill, P. M. W.; Pople, J. A. *Int. J. Quantum Chem.* **1991**, *40*, 745−772.
(39) Schafer, A.; Horn, H.; Ahlrichs, R. *J. Chem. Phys.* **1992**, *97*, 2571−2577.
(40) The simulation program was written in the Java language by B. Herreros and G. Harbison at the University of Nebraska-Lincoln. It is available at http://chemmac1.usc.edu/bruno/java/MAS.html.

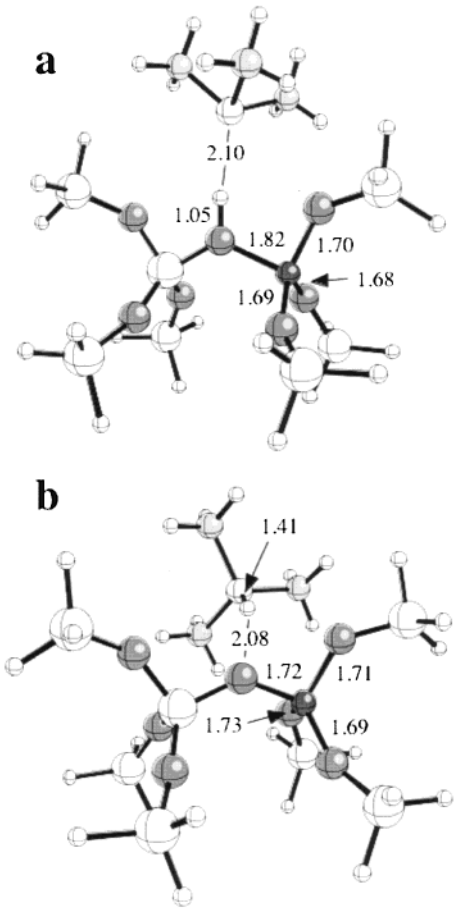

Figure 2. B3LYP/DZVP2 optimized geometries of the two $P(CH_3)_3$ complexes with the zeolite model. (a) $(CH_3)_3P{\cdot}HZ$, neutral $P(CH_3)_3$ in contact with the zeolite acid site. (b) $(CH_3)_3PH^+{\cdot}Z^-$, protonated $P(CH_3)_3$ complexed with the zeolite anion. Selected distances in Å are shown.

optimized geometry for the zwitterionic cluster, $(CH_3)_3PH^+{\cdot}Z^-$, in which the proton has transferred to $P(CH_3)_3$. This geometry is 5.5 kcal/mol lower in energy than the neutral cluster presented in 2a. Thus, this geometry should be greatly preferred and should correspond to the state experimentally observed. The O−H bond length is 2.08 Å. The P−H bond distance of 1.41 Å compares to a predicted value of 1.40 Å for bare $HP(CH_3)_3^+$ optimized at the same level of theory. The hydrogen bond energy is 16.5 kcal/mol, even more consistent with a strong hydrogen bond. The only unusual aspect of the optimized geometry is P−H−O angle of 147.6°. We expect these angles to be close to linear in strong hydrogen bonds. The Al−O distance is 1.72 Å, the same as the bond distance in the bare zeolite. Table 1 summarizes the four Al−O bond distances for all of the complexes reported. The Table also reports the root-mean-square deviations (RMSD) from the average of the four bond distances for each of the complexes. This value is one convenient metric of the degree of geometrical distortion around Al; it is greatest for the bare zeolite and decreases upon complexation to an extent that tracks the proton affinity of the base and, hence, the degree of proton transfer.

Theoretical Quadrupole Parameters. Table 1 also reports the quadrupolar coupling constants (Q_{cc}) and asymmetry parameters (η) for these complexes at both the RHF and density functional (B3LYP) levels. All calculated Q_{cc} values were actually negative, but the sign of this quantity does not affect our calculated line shapes. For convenience we treat Q_{cc} as an absolute value in all that follows. We focus on the B3LYP values, which are within ca. 10% of those obtained with neglect of correlation. As expected, the largest $|Q_{cc}|$ value (19.6 MHz) was determined for the protonated zeolite cluster in the absence of adsorbate. Hydrogen bonding without appreciable proton transfer reduced this value to only ca. 15 to 16.5 MHz. In the pyridine complex where appreciable proton transfer occurred, Q_{cc} decreased to 7.1 MHz, approaching the value calculated for the anionic zeolite cluster without any adsorbate, 5.1 MHz. The two stable states calculated for trimethylphosphine on the zeolite (Figure 2) were a study in contrasts. Table 1 shows that the complex without proton transfer, $(CH_3)_3P{\cdot}HZ$, had an appreciable value for the RMSD, 0.1018 Å, and a Q_{cc} of 15.3 MHz. $(CH_3)_3PH^+{\cdot}Z^-$ on the other hand had nearly identical Al−O distances (RMSD of 0.0258 Å) and a Q_{cc} of only 4.7 MHz, the smallest value in the table. For comparison we also optimized the geometry of a cluster modeling a hypothetical zeolite anion site with no cation or adsorbate, and RMSD in this case was 0.0159 Å.

Theoretical ^{27}Al Shieldings. Table 1 also reports isotropic ^{27}Al absolute shieldings calculated for the cluster models at the RHF level (i.e., with neglect of electron correlation). Remarkably, these values all fall within a 3.4-ppm range, and the correlation with degree of proton transfer (small as it is) trends counter to intuition. The largest shielding difference is between the zeolite without adsorbate and the zeolite complexed with nitromethane, the weakest base studied. The two theoretical minima for the zeolite complexed with trimethylphoshine, with and without proton transfer, have ^{27}Al isotropic shifts that differ by only 0.2 ppm. While the absolute values of these shieldings will change with inclusion of electron correlation or use of larger basis sets, the essential result, that the ^{27}Al chemical shift is almost completely insensitive to proton transfer, will not.

Simulated MAS Line Shapes. The calculated Q_{cc} and η values we used in numerical simulations of the MAS line shapes of the central transitions at a field strength of 8.46 T (93.7 MHz for ^{27}Al). Figure 3 reports these results for the two calculated states of $P(CH_3)_3$ on the zeolite as well as for the zeolite without adsorbate. The calculated line shape for the $(CH_3)_3PH^+{\cdot}Z^-$ complex is quite narrow, with a full width at half-height of only 1.3 kHz. In contrast, the $(CH_3)_3P{\cdot}HZ$ complex is predicted to have a very broad line showing an appreciable quadrupolar shift. This result is also plotted with an intensity normalized to provide a total integrated area identical to that in the plot for the $(CH_3)_3PH^+{\cdot}Z^-$ complex. In the case of the zeolite without any adsorbate the simulated MAS line shape is so broad that detection using a standard single-pulse and acquire sequence would be very challenging. Indeed, the experimental spectrum of the bare zeolite (also shown) reveals no hint of the ^{27}Al resonance. The noise level shown for the experimental spectrum of the bare zeolite was set by reference to an experimental spectrum of the $(CH_3)_3PH^+{\cdot}Z^-$ complex (vide infra) which was adjusted to have a peak height similar to that for its corresponding simulated spectrum. The expected intensities in the no-adsorbate case are below the experimental detection limit.

Figure 4 compares the simulated MAS line shapes of the zeolite complexes of nitromethane, acetone, and pyridine (Py) with that of the $(CH_3)_3PH^+{\cdot}Z^-$ complex; all are shown normalized to a constant integrated intensity. Only the $PyH^+{\cdot}Z^-$ and

Table 1. Experimental Proton Affinities (kcal/mol) of the Adsorbates, Predicted Al−O Bond Lengths and RMSD (Å), Predicted Quadrupolar Coupling Constants (MHz) and Asymmetry Parameters at the B3LYP/tzplarge//B3LYP/DZVP2 and RHF/tzplarge//B3LYP/DZVP2 Levels

complex	PA kcal/mol	Al–O_1 Å	Al–O_2 Å	Al–O_3 Å	Al–O_4 Å	RMSD[a] Å	B3LYP Q_{cc}[b]	B3LYP η	RHF Q_{cc}[b]	RHF η	^{27}Al σ ppm[c]
HZ		1.827	1.689	1.683	1.676	0.1253	19.63	0.156	21.23	0.140	532.5
CH_3NO_2·HZ	180	1.817	1.695	1.689	1.682	0.1115	16.54	0.147	17.89	0.123	535.9
CH_3COCH_3·HZ	193	1.805	1.694	1.688	1.684	0.1010	15.20	0.133	16.55	0.115	535.2
PyH^+·Z^-	222	1.743	1.704	1.689	1.712	0.0394	7.05	0.576	7.83	0.608	533.1
$(CH_3)_3P$·HZ	229	1.806	1.693	1.688	1.685	0.1018	15.31	0.138	16.82	0.122	534.6
$(CH_3)_3PH^+$·Z^-	229	1.722	1.714	1.692	1.725	0.0258	4.68	0.855	5.32	0.867	534.4
Z^-		1.715	1.700	1.722	1.713	0.0159	5.11	0.792	5.51	0.792	538.4

[a] Root-mean-square deviations of the four Al−O bond distances. [b] All Q_{cc} values in this investigation are negative. As the sign of this quantity does not affect the simulated spectra, absolute values are reported and discussed for convenience. [c] Absolute shieldings for ^{27}Al in the clusters, calculated at the RHF level.

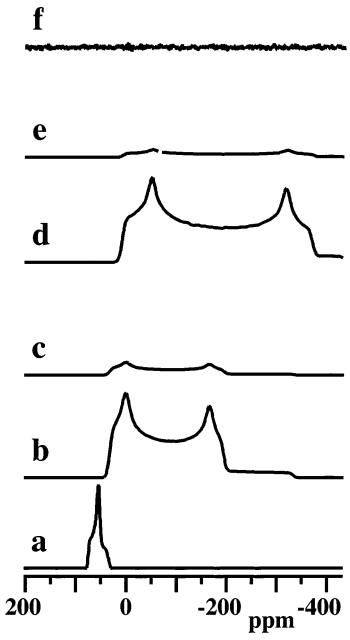

Figure 3. Calculated line shapes for the central transition of ^{27}Al under MAS (infinite spinning speed, 8.46 T) calculated using Q_{cc} and η values computed from the theoretical geometries for various zeolite−adsorbate complexes: (a) $(CH_3)_3PH^+$·Z^-; (b) $P(CH_3)_3P$·HZ, shown plotted so that its maximum intensity is the same as in a; (c) $(CH_3)_3P$·HZ, shown plotted with an integrated intensity identical to that in a; (d) zeolite HZSM-5 with no adsorbate, HZ, shown plotted so that its maximum intensity is the same as in a; (e) zeolite HZSM-5 with no adsorbate, HZ, shown plotted with an integrated intensity identical to that in a; (f) experimental spectrum of zeolite HZSM-5 with no adsorbate for comparison with e.

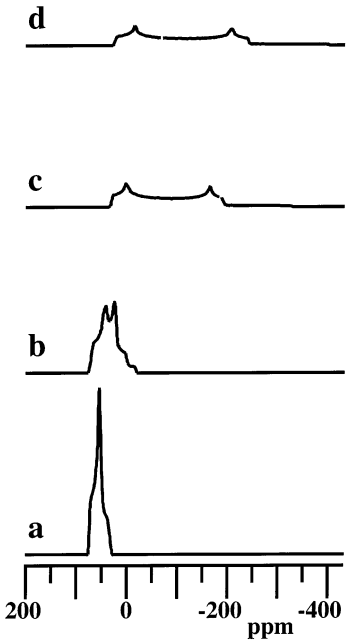

Figure 4. Calculated line shapes for the central transitions of ^{27}Al under MAS (infinite spinning speed, 8.46 T) calculated using Q_{cc} and η values computed from the theoretical geometries for various zeolite−adsorbate complexes, all shown normalized to the identical integrated intensities for comparison with experiment: (a) $(CH_3)_3PH^+$·Z^-, (b) PyH^+·Z^-, (c) CH_3COCH_3·HZ, (d) CH_3NO_2·HZ.

$(CH_3)_3PH^+$·Z^- complexes are predicted to have relatively narrow ^{27}Al lines, with the latter predicted to be somewhat narrower than the former.

NMR Experiments. Figure 5 presents experimental ^{27}Al MAS NMR spectra of the four complexes modeled theoretically in Figure 4. Adsorption of trimethylphosphine onto zeolite HZSM-5 produces a single sharp resonance at 52 ppm with a full width at half-maximum of 750 Hz. The line observed with pyridine was only slightly broader, 1.0 kHz. With acetone or nitromethane, much weaker bases, the ^{27}Al MAS spectra of the zeolite were so broad as to be almost featureless. A very low-intensity signal was reproducibly observed with acetone, while an analogous feature could be discerned for some, but not all samples of nitromethane on HZSM-5. Samples of acetone on HZSM-5 that were allowed to reach room temperature also gave a narrow ^{27}Al resonance (not shown). ^{13}C MAS NMR spectra confirmed that these samples had reacted to form mesityl oxide.[7] ^{27}Al MQMAS NMR spectra were also obtained for the zeolite complexes of trimethylphosphine and pyridine. These were each a single very sharp signal, and no additional features were resolved beyond what was observed with MAS alone. We were unable to observe MQMAS spectra for the other complexes as a result of the inefficiency of multiple quantum excitation for ^{27}Al environments with large quadrupole coupling constants.

Discussion

The agreement between experiment and theory obtained in this study is very encouraging. The two complexes with significant proton transfer from the zeolite to the base were predicted to give narrow ^{27}Al MAS resonances, as was confirmed experimentally. In the case of trimethylphosphine, where two stable states were obtained theoretically, agreement between experiment and simulation was obtained only for the lower-energy state, as expected. The nitromethane and acetone complexes were predicted to have appreciably less proton transfer,

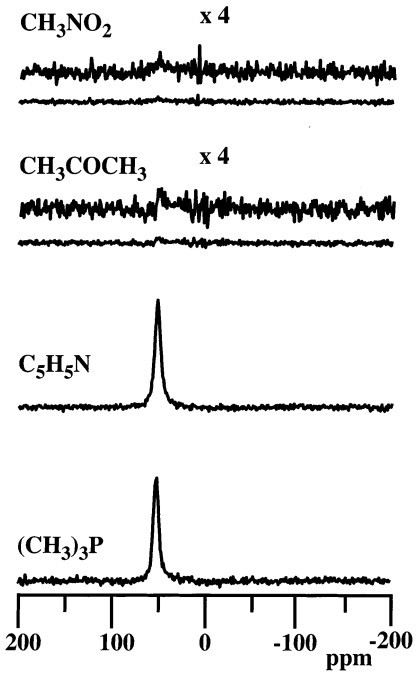

Figure 5. ^{27}Al MAS NMR (93.7 MHz) spectra of zeolite HZSM-5 with various adsorbates as indicated. All spectra were measured at 298 K with the exception of the acetone complex which was measured at 153 K to prevent reaction to form mesityl oxide, a stronger base. The spinning speed was 7.2 kHz in each case.

leading to much broader spectra, and these indeed were too broad to be characterized in our experiments.

The experimental spectra of the trimethylphosphine and pyridine complexes of the zeolite are somewhat narrower than those simulated using theoretical quadrupole parameters for the $(CH_3)_3PH^+ \cdot Z^-$ and $PyH^+ \cdot Z^-$ complexes, and the fine structure predicted in the latter case was not evident in the experimental spectrum. Our intuition is that more accurate agreement between experiment and theory might require structural models much larger than those used here, to incorporate long-range electrostatic effects and structural relaxation. For example, zeolite ZSM-5 is known to undergo a phase transition from monoclinic to orthorhombic upon adsorption of *p*-xylene,[41] and this subtle effect cannot be reproduced using clusters smaller than a unit cell. More importantly, the theoretical calculations correspond to a single geometric state at 0 K, whereas the experiment includes significant thermal averaging. Thus, it is not surprising that our experimental (298 K) line shapes are somewhat narrower than those predicted by theory.

Bryant et al. used both plane wave density functional calculations and embedded cluster methods to calculate ^{27}Al EFG data for the mineral andalusite.[42] Although they found the full-crystal plane wave calculations were needed for accurate orientations of the EFG tensors, the cluster calculations provided good agreement with experiment for both Q_{cc} and η. Koller et al. also used cluster models and DFT to theoretically calculate quadrupolar parameters for an isolated zeolite acid site, as well as clusters complexed to acetonitrile, methanol, and ammonia.[24] Acetonitrile is a weak base with a proton affinity of 186 kcal/mol, placing it intermediate between nitromethane and acetone. Those workers calculated a Q_{cc} value for their zeolite acid site cluster of 18.2 MHz, and saw this value reduced to 13.5 MHz upon adsorption of acetonitrile. Koller predicted much larger reductions in Q_{cc} upon complexation with either methanol or ammonia, each of which formed cooperative hydrogen bonds with the acid site. Formation of two or more hydrogen bonds between the adsorbed base and the zeolite Brønsted site is known to assist proton transfer. It is well established that ammonia is protonated on zeolites despite an intermediate proton affinity (204 kcal/mol) as a result of this cooperative hydrogen bonding.

Several of us have published on the theory of persistent carbenium ions in acidic zeolites.[43,44] In its simplest form,[43] this theory considers proton transfer from a zeolite Brønsted site to an adsorbed olefinic or aromatic hydrocarbon. We found that proton transfer occurs to form a carbenium ion that persists indefinitely at room temperature only for hydrocarbon bases with gas-phase proton affinities of ca. 209 kcal/mol or higher. Both $P(CH_3)_3$ (229.2 kcal/mol) and Py (222 kcal/mol) lie above this limit, while acetone (194 kcal/mol) and nitromethane (180.4 kcal/mol) lie below. Acetylacetone has sometimes been adsorbed onto zeolites for the purpose of visualizing ^{27}Al resonances.[45] This has usually been done for extra-lattice sites formed by steaming, but framework sites associated with Brønsted sites are also seen using this procedure, even when acetylacetone is adsorbed from the gas phase. We did not consider that base in our investigation, but we note that its gas-phase proton affinity, 208.8 kcal/mol, is at the lower limit for proton transfer that we previously estimated for hydrocarbon bases. The ca. 209 kcal/mol threshold for proton transfer also explains the line-narrowing effect of acetone adsorption at room temperature or above. The experimental ^{27}Al MAS spectrum of acetone on zeolite HZSM-5 shown in Figure 5 was measured at a temperature of 153 K for a sample prepared by adsorption and handling at 193 K. This spectrum shows the ^{27}Al line width to be too broad for detection using single-pulse excitation and MAS averaging, as predicted theoretically. However, a narrow ^{27}Al resonance was observed when this and similar samples were allowed to warm to 298 K in the MAS probe or when then acetone was adsorbed at 298 K (not shown). Following previous work[8] we used ^{13}C MAS NMR to monitor a sample of acetone-2-^{13}C on HZSM-5. Below room temperature the ^{13}C spectrum showed an adsorption complex of acetone on the Brønsted site, and when this sample was warmed to 298 K, the ^{13}C spectrum showed that much of the acetone had dimerized and dehydrated to form mesityl oxide. Mesityl oxide has a gas-phase proton affinity of 210.0 kcal/mol. We earlier reported the B3LYP geometry of mesityl oxide on a zeolite HZSM-5 cluster model;[23] that structure shows the proton almost exactly intermediate between the zeolite and the base, and it shows considerable relaxation of the environment around aluminum.

MQMAS experiments did not reveal any additional aluminum sites beyond those seen with MAS. TRAPDOR[46] or similar experiments may prove useful in future work.

(41) Fyfe, C. A.; Strobl, H.; Kokotailo, G. T.; Kennedy, G. J.; Barlow, G. E. *J. Am. Chem. Soc.* **1988**, *110*, 3373−3380.
(42) Bryant, P. L.; Harwell, C. R.; Wu, K.; Fronczek, F. R.; Hall, R. W.; Butler, L. G. *J. Phys. Chem.* **1999**, *103*, 5246−5252.
(43) Nicholas, J. B.; Haw, J. F. *J. Am. Chem. Soc.* **1998**, *120*, 11804−11805.
(44) Song, W.; Nicholas, J. B.; Haw, J. F. *J. Am. Chem. Soc.* **2001**, *123*, 121−129.
(45) Alexander, S. M.; Bibby, D. M.; Howe, R. F.; Meinhold, R. H. *Zeolites* **1993**, *13*, 441−447.
(46) Grey, C. P.; Vega, A. J. *J. Am. Chem. Soc.* **1995**, *117*, 8232−8242.

Conclusions

The ^{27}Al isotropic chemical shift of the Brønsted acid site of a zeolite is almost entirely insensitive to proton transfer to an adsorbed base. However, the quadrupolar coupling constant Q_{cc} is very sensitive to proton transfer as a result of geometric relaxation from a trigonally distorted tetrahedron to a more-perfect tetrahedral geometry. As a result, the MAS NMR line width of the central ($+^1/_2 \rightleftarrows -^1/_2$) transition reports whether proton transfer occurs upon adsorption of a base. The threshold for proton transfer, and hence narrowing of the central transition of the ^{27}Al resonance under MAS conditions, occurs near the 209 kcal/mol gas-phase value previously estimated for hydrocarbon adsorbates from studies of carbenium ions in zeolites.[43] The ^{27}Al line width provides an independent measure of proton transfer, and we suggest that it be applied as a referee method where consensus cannot be reached on the basis of other spectroscopic measurements of proton transfer from solid acids to adsorbed bases.

Acknowledgment. This work was supported by the National Science Foundation (CHE-9996109). Computer resources were provided by the National Energy Research Supercomputer Center (NERSC), Berkeley, CA.

JA012336U